International Journal of Bifurcation and Chaos, Vol. 13, No. 4 (2003) 843–861

STICK-SLIP DYNAMICS OF A TWO-DEGREE-OF-FREEDOM SYSTEM

J. AWREJCEWICZ and P. OLEJNIK
Technical University of Łódź,
Department of Automatics and Biomechanics (K-16),
1/15 Stefanowskiego St., 90-924 Łódź, Poland

Received January 5, 2001; Revised January 4, 2002

Two-degree-of-freedom autonomous system with friction is analyzed numerically. The friction coefficient has been smoothened using arc tan function. The standard, but slightly modified chaos identification tools have been applied for the analyzed discontinuous system. Some interesting examples of stick-slip regular and chaotic dynamics have been illustrated and discussed.

Keywords: Friction; stick-slip dynamics; bifurcation; chaos; Lyapunov exponents.

1. Introduction

In spite of the fact that there are many papers devoted to investigations of regular and chaotic dynamics of mechanical systems with friction it seems that up to now not all the possible nonlinear phenomena have been properly understood or even detected and explained [Awrejcewicz 1996; Awrejcewicz & Delfs, 1990a, 1990b; Brogliato, 1996; Deimling & Szilágyi, 1994; Galvanetto *et al.*, 1995; Kunze, 2000; Monteiro, 1994; Oden & Martins, 1985].

This paper is devoted to numerical investigations, but the problem is expected to be attacked also from an analytical point of view. The stick-slip chaos has been predicted analytically using the Melnikov technique by Awrejcewicz and Holicke [1999], but such a prediction for two-degree-of-freedom system is in general more complicated and probably impossible for multibody dynamical systems. Even if this problem will be solved it will contain only special type of nonlinearities, and it will be valid only for special systems. Therefore, we have focused here on numerical simulations, which do not include the mentioned drawbacks.

We use a similar approach by the introduction of an arc tan instead of sgn [Van de Vrande *et al.*, 1999]. This approximation is especially useful during calculations of the Lyapunov exponents where a similar approach to Oseledec [1968] can be applied.

Our results show that it is very difficult to apply directly the method used by Pratt and Williams [1981], and in agreement with the work of Van de Vrande [1999] we show some benefits of the used smoothing function. In addition, we have demonstrated some of the interesting discontinuous behavior of nonlinear dynamics of our coupled self-excited oscillators with friction.

2. Analyzed System and Friction

The analyzed system with two-degree-of-freedom [Olejnik, 2000] is shown in Fig. 1.

Two masses move along the coordinates X_1, X_2 due to the friction forces F_1, F_2 occurring between them and the belt that moves with constant velocity. As usual, the constant stiffness coefficients are denoted by k_i, $i = 0, 1, 2$, whereas damping coefficients are denoted by c_j, $j = 1, 2$. The friction static forces F_i, $i = 1, 2$ are defined by

$$F_{s,i} = \mu_0 F_{N,i} \quad i = 1, 2, \tag{1}$$

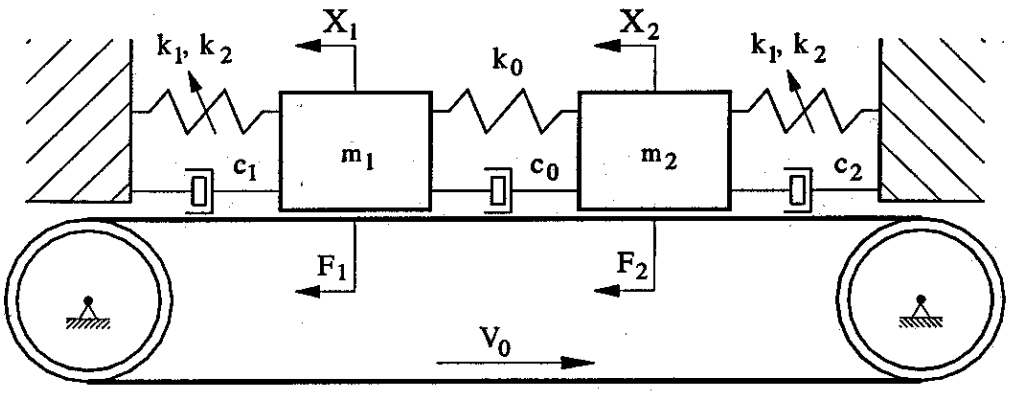

Fig. 1. The considered system.

where $F_{N,i} = m_i g$ is the pressing force generated by the mass m_i $(i = 1, 2)$, and μ_0 is the value of the static force coefficient.

The dynamic friction forces are governed by the equations

$$F_i = -\mu F_{N,i} \operatorname{sgn} v_{w,i} = -\frac{\mu F_{s,i}}{\mu_0} \operatorname{sgn} v_{w,i}, \tag{2}$$

where $v_{w,i} = \dot{x}_i - V_0$ is the relative velocity, static μ_0 and dynamic μ friction coefficients. The relation between static and dynamic coefficients is introduced in the following way:

$$\mu = \frac{\mu_0}{1 + \delta |v_{w,i}|}. \tag{3}$$

Above, δ coefficient characterizes the dynamic coefficient decrease which accompanies an increase of the relative velocity. The static forces occur when the relative velocity is equal to zero. Therefore, one gets

$$\begin{cases} |F_i| \le F_{s,i} & v_{w,i} = 0, \\ F_i = -\operatorname{sgn} v_{w,i} \dfrac{F_{s,i}}{1 + \delta |v_{w,i}|} & v_{w,i} = 0, \end{cases} \tag{4}$$

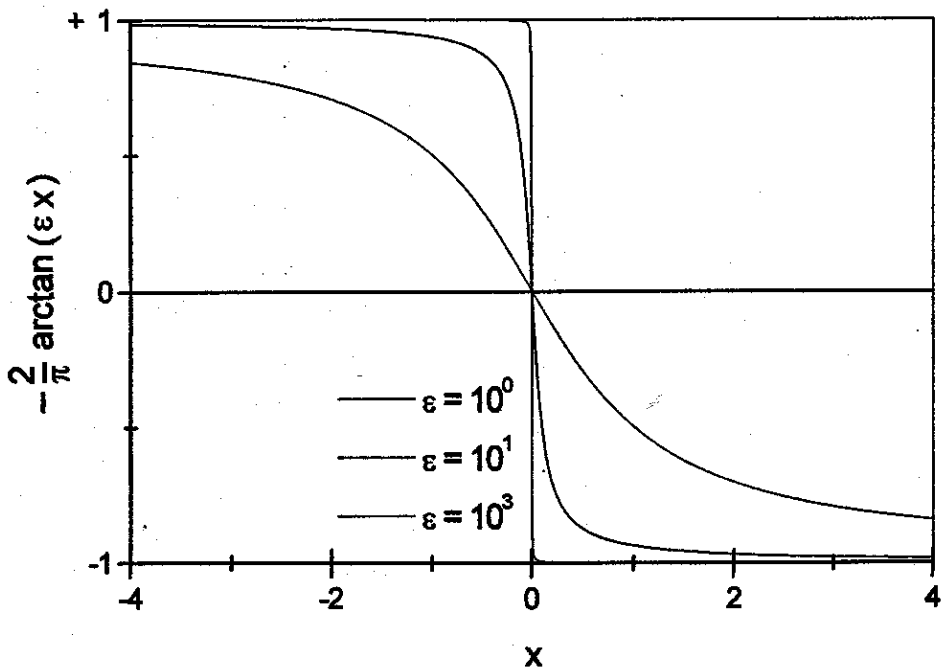

Fig. 2. Influence of ε for the approximation given in Eq. (5).

where $F_{s,i}$ $(i = 1, 2)$ are defined by Eq. (1). The following approximation to the sgn function is applied

$$\operatorname{sgn}(v_{w,i}) = \frac{2}{\pi}\arctan(\varepsilon v_{w,i}), \tag{5}$$

where $\varepsilon > 0$. The estimation of Eq. (5) is shown in Fig. 2. It is seen that for $\varepsilon = 10^3$ arctan almost exactly describes the properties of the function sgn. Taking into account Eq. (5) we get

$$F_i = -\frac{2}{\pi}\frac{F_{s,i}\arctan(\varepsilon v_{w,i})}{(1+\delta|v_{w,i}|)}, \quad i = 1, 2, \tag{6}$$

which is further used.

The following nondimensional equations govern dynamics of our two bodies dynamical system

$$\begin{aligned}
&\xi_1\ddot{y}_1+\alpha_0(\dot{y}_1-\dot{y}_2)+\alpha_1\dot{y}_1+(1+\beta_1)y_1-\beta_2 y_1^3-y_2 \\
&\quad=-\frac{2\arctan(\varepsilon\overline{v}_{w,1})}{\pi(1+\gamma|\overline{v}_{w,1}|)}, \\
&\xi_2\ddot{y}_2-\alpha_0(\dot{y}_1-\dot{y}_2)+\alpha_2\dot{y}_2+(1+\beta_1)y_2-\beta_2 y_2^3-y_1 \\
&\quad=-\frac{2\beta\arctan(\varepsilon\overline{v}_{w,2})}{\pi(1+\gamma|\overline{v}_{w,2}|)}.
\end{aligned} \tag{7}$$

The relations between physical values of parameters, coordinates and time, and their nondimensional adequate are as follows: $\xi_i = m_i\omega_1^2/k_0$, $\alpha_j = c_j\omega_1/k_0$, $\beta_1 = k_1/k_0$, $\gamma = F_{s,1}\delta/\sqrt{k_0 m_1}$, $\overline{V}_0 = \sqrt{k_0 m_1}V_0/F_{s,1}$, $\overline{v}_{w,i} = \dot{y}_i - \overline{V}_0$, $\beta = F_{s,2}/F_{s,1}$, $\beta_2 = k_2 F_{s,1}^2/k_0^3$, $i = 1, 2$, $j = 0, 1, 2$. An introduction of dimensionless quantities has led to the reduction of the parameters from 13 to 11.

3. An Overview of the Methods of Analysis

3.1. *Time histories*

One has to realize that using numerical methods, we only get an approximation of the real true trajectories of a system being analyzed due to the finite step of the numerical integrations and finite accuracy of the numbers used in the floating-point arithmetic. Nevertheless, the numerical approximations are suitable for engineering purposes when they are properly applied which is important for our discontinuous system.

It is clear that a duration of a transitional process depends on initial conditions and the system parameters. Here we discuss this problem in more detail on the basis of a few computational examples related to Eqs. (7). In Fig. 3, a coordinate versus time is presented for $t = 0$. In this case, the masses are in the equilibrium positions, whereas their initial velocities are equal to the belt velocity. In practice, the system from the beginning starts to move on an attractor. When the initial conditions are changed, a transitional process occurs of a duration equal to $t = 4$ (see Fig. 4). Our numerical analysis shows that in some cases the transitional state can be even 10 times larger.

In both previously discussed cases, we have dealt with the periodic attractor. A situation changes dramatically if a strange chaotic attractor appears. For this case it is rather difficult to define the beginning of observation, and therefore the first hundred "periods" of oscillations are neglected. The corresponding example is given in Fig. 5. It is seen from both Figs. 4 and 5 that a decreasing part of time histories is more steep than an increasing part. This is a typical behavior of our stick-slip system with friction. The first mentioned part corresponds to a slip, whereas the second one (slower) to a stick between a mass and the tape.

3.2. *Phase spaces*

The analyzed set of equations is transformed to the following one

$$\begin{cases}
\dfrac{d\tilde{x}_1}{d\tau} = \tilde{x}_2, \\
\dfrac{d\tilde{x}_2}{d\tau} = \dfrac{1}{\xi_1}\left(-\dfrac{2}{\pi}\dfrac{\arctan(\varepsilon\tilde{v}_{w,1})}{(1+\gamma|\tilde{v}_{w,1}|)} - \alpha_0\tilde{x}_2 + \alpha_0\tilde{x}_4 - \alpha_1\tilde{x}_2 - (1+\beta_1)\tilde{x}_1 + \beta_2\tilde{x}_1^3 + \tilde{x}_3\right), \\
\dfrac{d\tilde{x}_3}{d\tau} = \tilde{x}_4, \\
\dfrac{d\tilde{x}_4}{d\tau} = \dfrac{1}{\xi_2}\left(-\dfrac{2\beta}{\pi}\dfrac{\arctan(\varepsilon\tilde{v}_{w,2})}{(1+\gamma|\tilde{v}_{w,2}|)} + \alpha_0\tilde{x}_2 + \alpha_0\tilde{x}_4 - \alpha_2\tilde{x}_4 - (1+\beta_1)\tilde{x}_3 + \beta_2\tilde{x}_3^3 + \tilde{x}_1\right),
\end{cases} \tag{8}$$

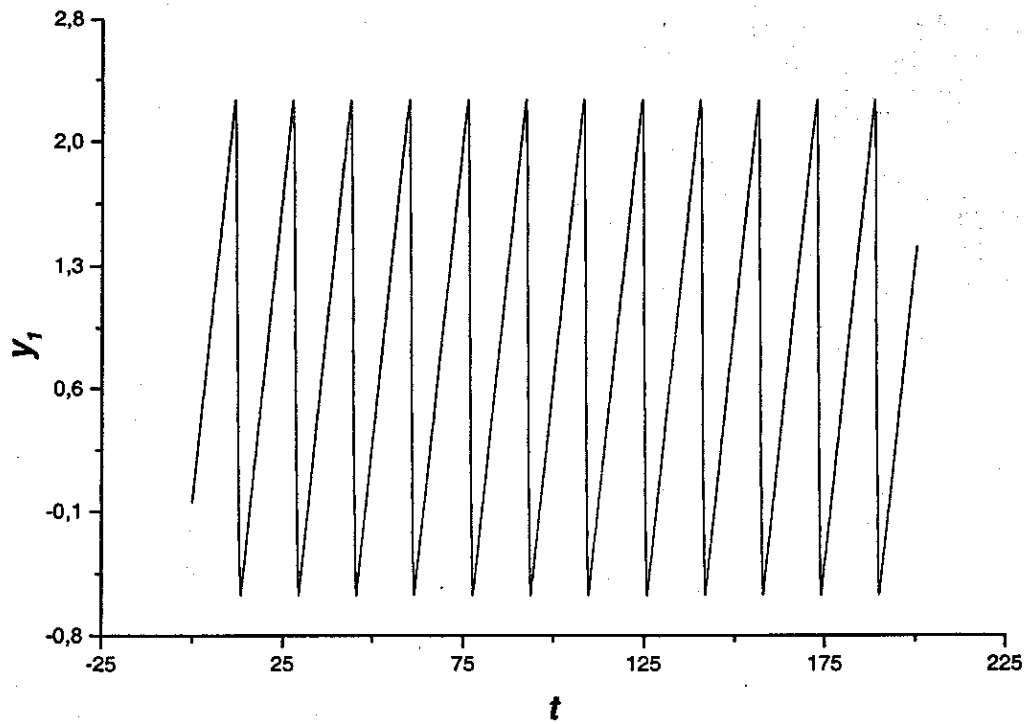

Fig. 3. Time history of displacement y_1 with very short transitional process for the parameters: $\gamma = 3$, $\beta = 1$, $V_0 = 0.2$, $\alpha_0 = \alpha_1 = \alpha_2 = 0$, $\beta_1 = \beta_2 = \xi_1 = \xi_2 = 0.1$, and the initial conditions: $y_1 = y_2 = 0$, $\dot{y}_1 = \dot{y}_2 = 0.2$.

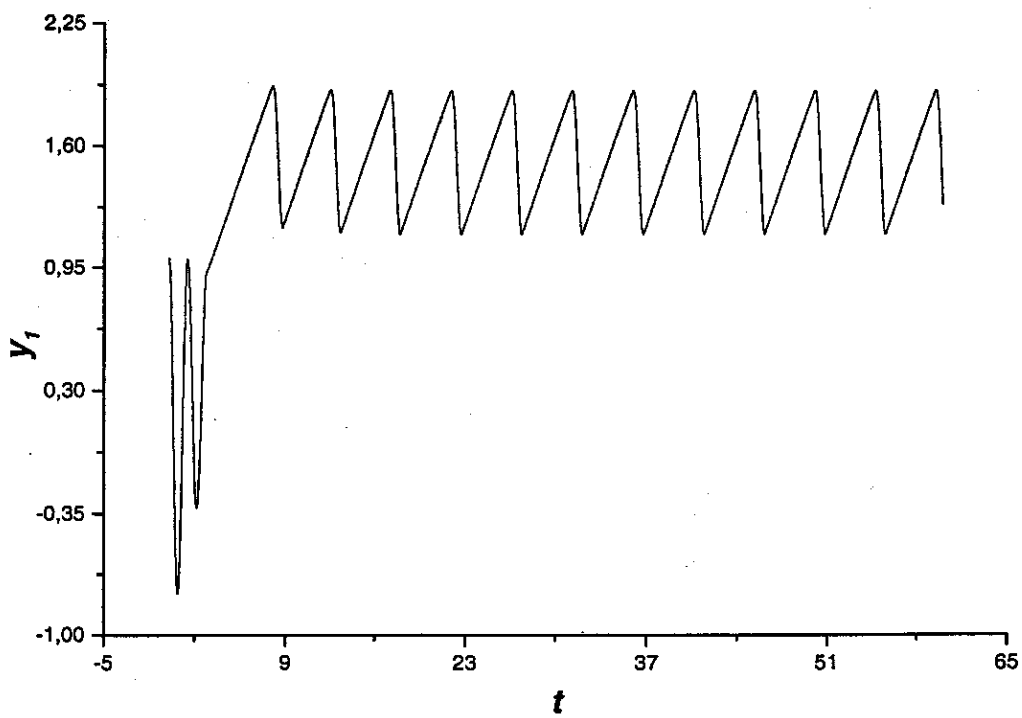

Fig. 4. Time history of displacement y_1 (with a clearly visible transitional process) for the initial conditions: $y_1 = y_2 = 1$, $\dot{y}_1 = \dot{y}_2 = 0.2$ (other parameters are the same as in Fig. 3).

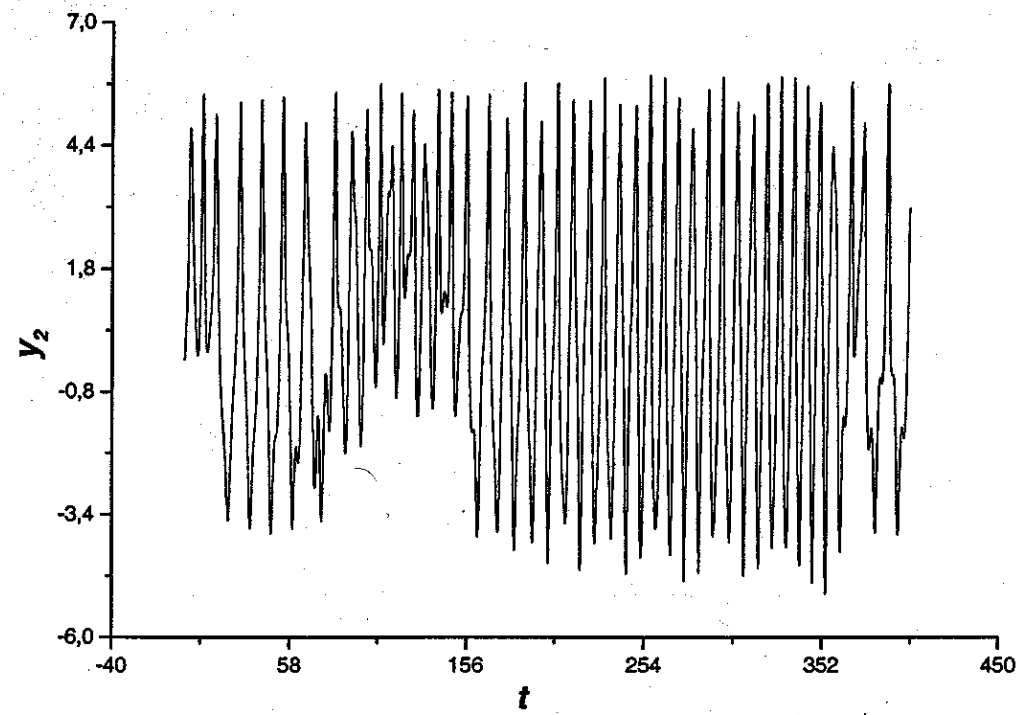

Fig. 5. Chaotic time history of $y_2(t)$ for the parameters: $\gamma = 0.03$, $\beta = 1$, $V_0 = 5$, $\alpha_0 = 0.01$, $\alpha_1 = 0$, $\alpha_2 = 0.03$, $\beta_1 = 1$, $\beta_2 = 0.1$, $\xi_1 = 1.12$, $\xi_2 = 1$, and the initial conditions: $y_1 = 0.4$, $y_2 = -0.12$, $\dot{y}_1 = -0.56$, $\dot{y}_2 = 0.12$.

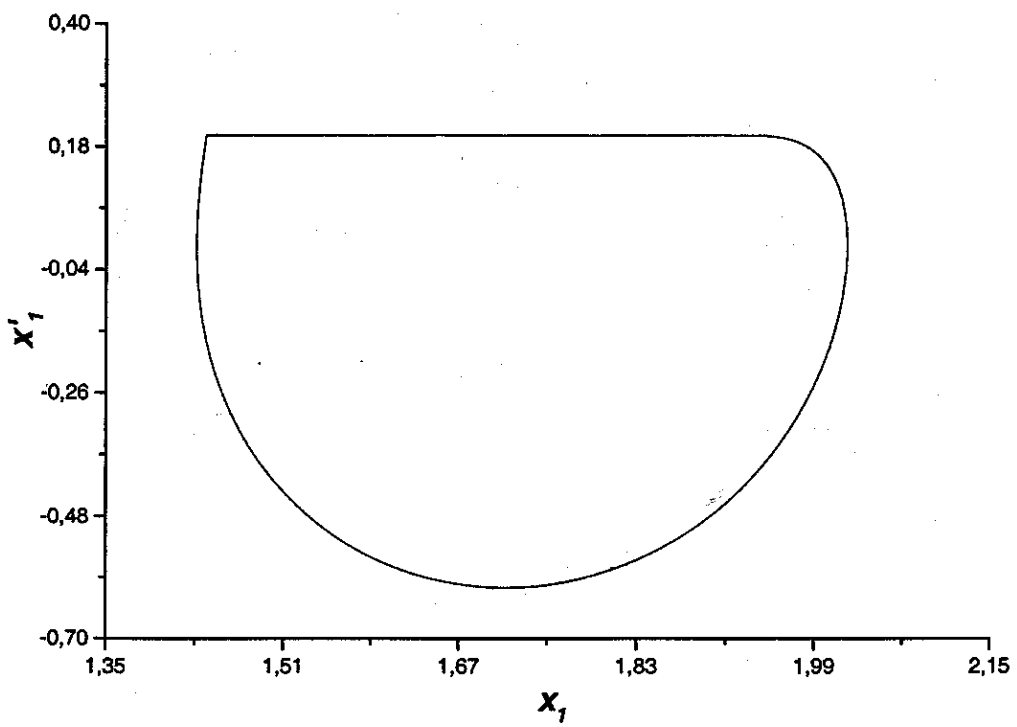

Fig. 6. Phase plane $\dot{x}_1(x_1)$ of the periodic motion for the parameters: $\gamma = 3$, $\beta = 1$, $V_0 = 0.2$, $\alpha_0 = \alpha_1 = \alpha_2 = 0$, $\beta_1 = \beta_2 = 0.1$, $\xi_1 = \xi_2 = 0.5$, and the initial conditions: $x_1 = x_2 = 0$, $\dot{x}_1 = \dot{x}_2 = 0.2$.

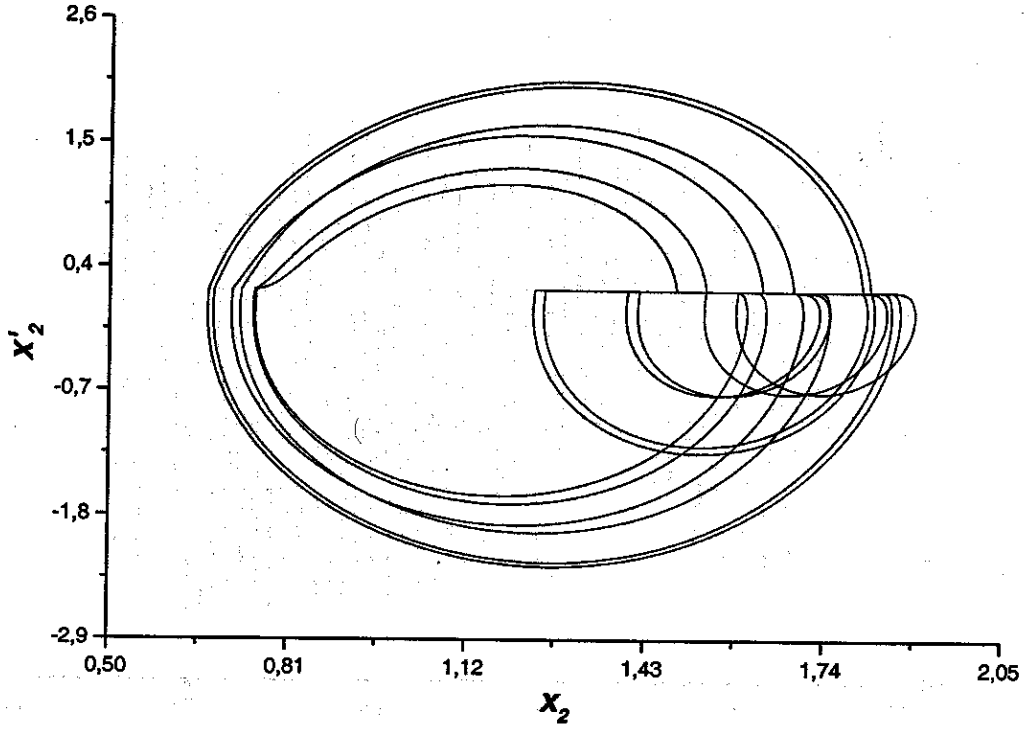

Fig. 7. Phase plane $\dot{x}_2(x_2)$ during stick-slip chaos for the parameters: $\gamma = 3$, $\beta = 0.5$, $V_0 = 0.2$, $\alpha_0 = 0.1$, $\alpha_1 = \alpha_2 = 0$, $\beta_1 = \beta_2 = \xi_1 = \xi_2 = 0.1$, and the initial conditions: $x_1 = 0$, $x_2 = 0.12$, $\dot{x}_1 = \dot{x}_2 = 0$.

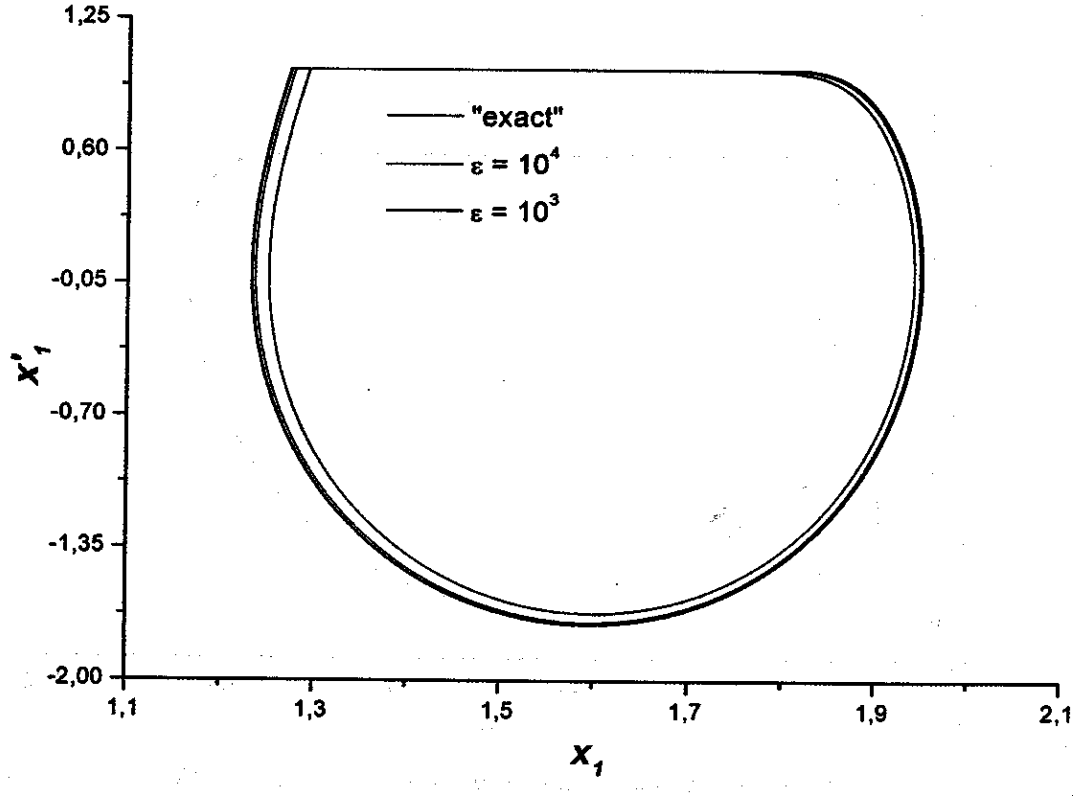

Fig. 8. Influence of ε on the results (parameters: $\gamma = 1$, $\beta = V_0 = 1$, $\alpha_0 = \alpha_1 = \alpha_2 = 0.02$, $\beta_1 = \beta_2 = \xi_1 = \xi_2 = 0.1$, and the initial conditions: $x_1 = x_2 = 0$, $\dot{x}_1 = \dot{x}_2 = 1$).

where $\tilde{v}_{w,i} = \tilde{x}_{2i} - \overline{V}_0$, $i = 1, 2$, $\tilde{x}_1 = y_1$, $\tilde{x}_2 = \dot{y}_1$, $\tilde{x}_3 = y_2$, $\tilde{x}_4 = \dot{y}_2$. For further considerations we take $\tilde{x}_j \equiv x_j$, $j = 1, \ldots, 4$, where now x_i correspond to the displacement of m_i, whereas $\dot{x}_i$ are the corresponding velocities ($i = 1, 2$).

A typical projection of a trajectory associated with our system with friction is shown in Fig. 6. Two parts are easy distinguishable: the stick part (where $\dot{x}_1 = V_0 = 0.2$, which is represented by the horizontal line) and the slip part.

A more complicated motion is presented in Fig. 7. A time occurrence and a duration of a stick are unpredictable. The phases appear with different velocities, which are represented by small and large arcs in the phase plane. For small x_2 values (0.7–0.9) a stick does not occur when $\dot{x}_2 = V_0$. It means that the corresponding static friction force has been smaller than the absolute value of resulting horizontal forces [Awrejcewicz & Holicke, 1999; Awrejcewicz, 1996; Awrejcewicz & Mrozowski, 1989].

The phase planes can also be used for an error estimation during approximation of sgn by arctan. ε serves as the control parameter and the different periodic orbits for different ε values are shown in Fig. 8.

3.3. *Poincaré sections*

For our autonomous case, when $\dot{x}_1$ changes its sign, then a point corresponding to the mass m_2 is constructed on the Poincaré map.

In what follows, we are going to show that our autonomous system can exhibit stick-slip chaotic (Fig. 9), stick-slip periodic (Fig. 10) as well as stick-slip quasi-periodic dynamics (Fig. 11).

Because of the introduced symmetry, only a behavior of one mass has been presented.

3.4. *Bifurcation diagrams*

The bifurcation diagrams have been constructed in two ways. For instance, by changing a parameter in the interval (0.1, 0.5) with the step 0.001, we get 400 Poincaré maps. Then, one of the phase axes is taken and all results are presented versus the parameter. Another way is that for increasing parameter values we change the initial conditions, and contrary to the first case, we leave an attractor (in the previous case we were entirely on an attractor).

An example of bifurcation diagram is shown in Fig. 12.

Beginning from the smallest considered values of ξ_2 we observe different multiple periodic motion and period doubling bifurcations occur. In the interval $\xi_2 \in (0.5, 0.6)$ period-6 window appears. For $\xi_2 = 0.6$ and $x_2 \approx 1.0$ the saddle-node bifurcation occurs, and then other local classical bifurcations appear. For $\xi_2 \approx 0.9$ the period doubling bifurcation occur (with a decrease of the bifurcation parameter). This corresponds to a route to chaos and to a route from chaos to regular (periodic) behavior.

It should be emphasized that for $\xi_2 \approx 1.22$ a crisis between period-6 orbit and chaos occurs, and its enlargement is shown in Fig. 12(b). It is clearly seen how the successive period doubling (accompanying a decrease of ξ_2) leads to a periodic motion, which exists for $\xi_2 \in (1.15, 1.22)$.

3.5. *Lyapunov exponents*

The Lyapunov exponents have been estimated from Eq. (8) using standard calculating procedure [Wolf *et al.*, 1985].

In order to verify the developed code the well known Lorenz set of equations [see Eq. (9)] has been tested.

$$\begin{cases} \dot{x}_1 = -\sigma x_1 + \sigma x_2, \\ \dot{x}_2 = r x_1 - x_2 - x_1 x_3, \\ \dot{x}_3 = x_1 x_2 - b x_3. \end{cases} \tag{9}$$

In [Wolf *et al.*, 1985] for $\sigma = 16$, $r = 40$, $b = 4$ the following Lyapunov exponents have been computed: $L_1 = 1.37$, $L_2 = 0.00$, $L_3 = -22.37$. Using our method we have $L_1 = 1.36$, $L_2 = 0.00$, $L_3 = -22.37$ for $h = 2 \cdot 10^{-3}$, $dt = 4 \cdot 10^{-2}$, $k = 7 \cdot 10^3$. The computation process is illustrated in Fig. 13.

In order to judge about a strangeness of a chaotic attractor we introduce the following dimension

$$d_L = i + (\lambda_1 + \lambda_2 + \lambda_3)/|\lambda_4|, \tag{10}$$

where i is the index corresponding to a smallest non-negative Lyapunov exponent. For Lorenz system we have obtained $d_L = 2.06$.

Now we come back to our chaotic attractor presented in Fig. 9. For $h = 2 \cdot 10^{-3}$, $dt = 5 \cdot 10^{-2}$, $k = 2 \cdot 10^4$ the following Lyapunov exponents have been obtained: $L_1 = 0.20$, $L_2 = 0.09$, $L_3 = -0.10$, $L_4 = -0.29$. Therefore, the hyperchaotic strange stick-slip attractor has been detected for our system with friction ($d_L = 2.65$). The computation process in this case is illustrated in Fig. 14.

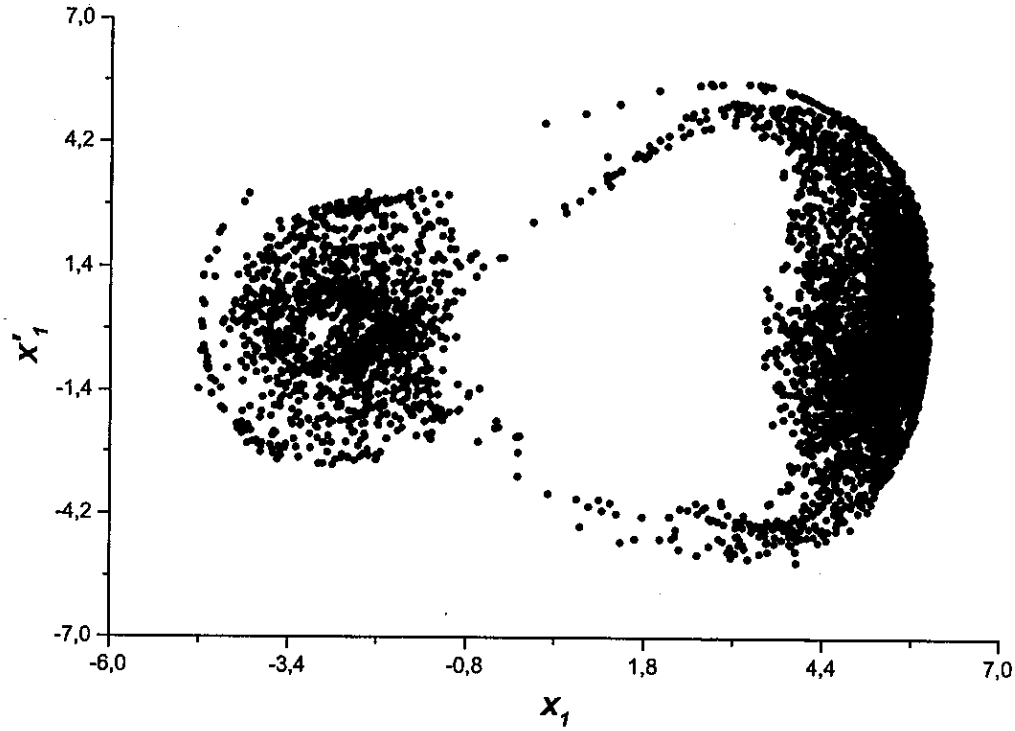

Fig. 9. Poincaré map $\dot{x}_1(x_1)$ for the parameters: $\gamma = 0.03$, $\beta = 1$, $V_0 = 5$, $\alpha_0 = 0.01$, $\alpha_1 = 0$, $\alpha_2 = 0.03$, $\beta_1 = 1$, $\beta_2 = 0.1$, $\xi_1 = 1.12$, $\xi_2 = 1$, and the initial conditions: $x_1 = 0.4$, $x_2 = -0.12$, $\dot{x}_1 = -0.56$, $\dot{x}_2 = 0.12$ (chaotic orbit).

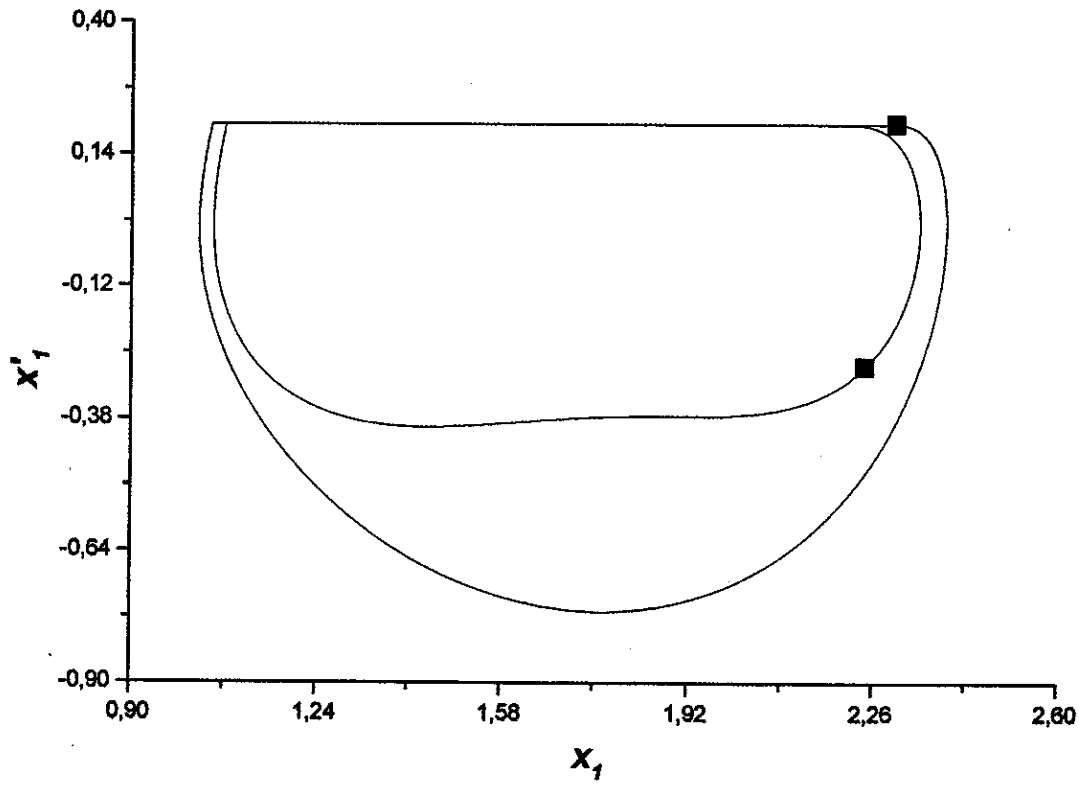

Fig. 10. Phase portrait and the corresponding Poincaré map (red squares) $\dot{x}_1(x_1)$ for the parameters: $\gamma = 3$, $\beta = 1$, $V_0 = 0.2$, $\alpha_0 = \alpha_1 = \alpha_2 = \beta_1 = \beta_2 = 0.1$, $\xi_1 = \xi_2 = 1$, and the initial conditions: $x_1 = x_2 = \dot{x}_1 = \dot{x}_2 = 0$ (periodic orbit).

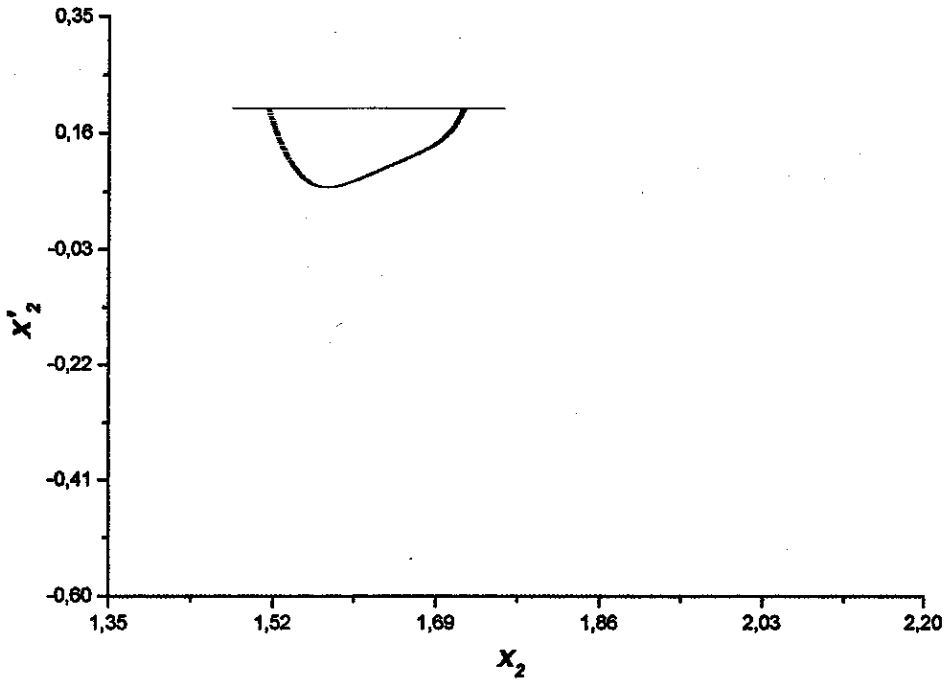

Fig. 11. Poincaré map $\dot{x}_2(x_2)$ for the parameters: $\gamma = 3$, $\beta = 1$, $V_0 = 0.2$, $\alpha_0 = \alpha_1 = \alpha_2 = 0$, $\beta_1 = \beta_2 = 0.1$, $\xi_1 = \xi_2 = 1$, and the initial conditions: $x_1 = -0.1$, $x_2 = 0.2$, $\dot{x}_1 = \dot{x}_2 = 0$ (quasi-periodic orbit).

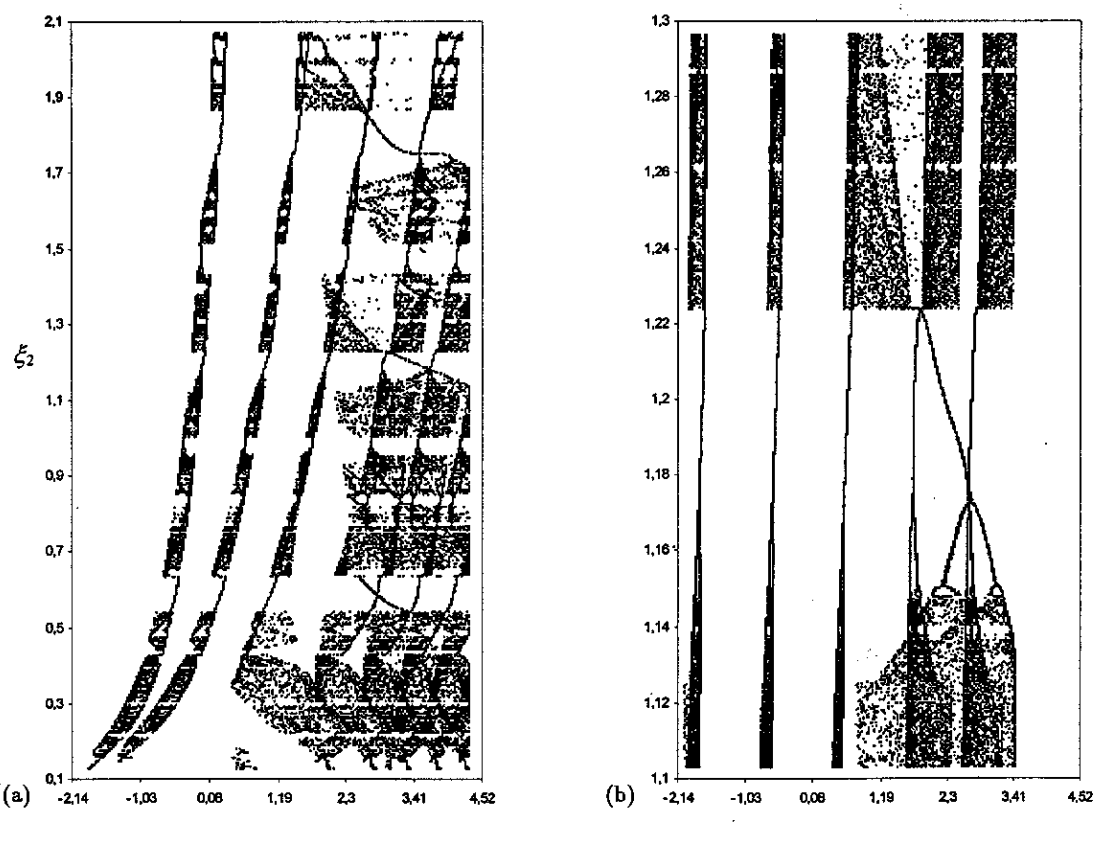

Fig. 12. Bifurcation diagram for the parameter ξ_2: (a) $\xi_2 \in (0.1, 2.1)$, (b) $\xi_2 \in (1.1, 1.3)$. The following parameters are fixed: $\gamma = 2.03$, $\beta = 21$, $V_0 = 0.2$, $\alpha_0 = 0.0045$, $\alpha_1 = 0.01$, $\alpha_2 = 0.19$, $\beta_1 = 0.12$, $\beta_2 = 0.2$. The initial conditions: $x_1 = -0.1$, $x_2 = 0.2$, $\dot{x}_1 = 0$, $\dot{x}_2 = 0$.

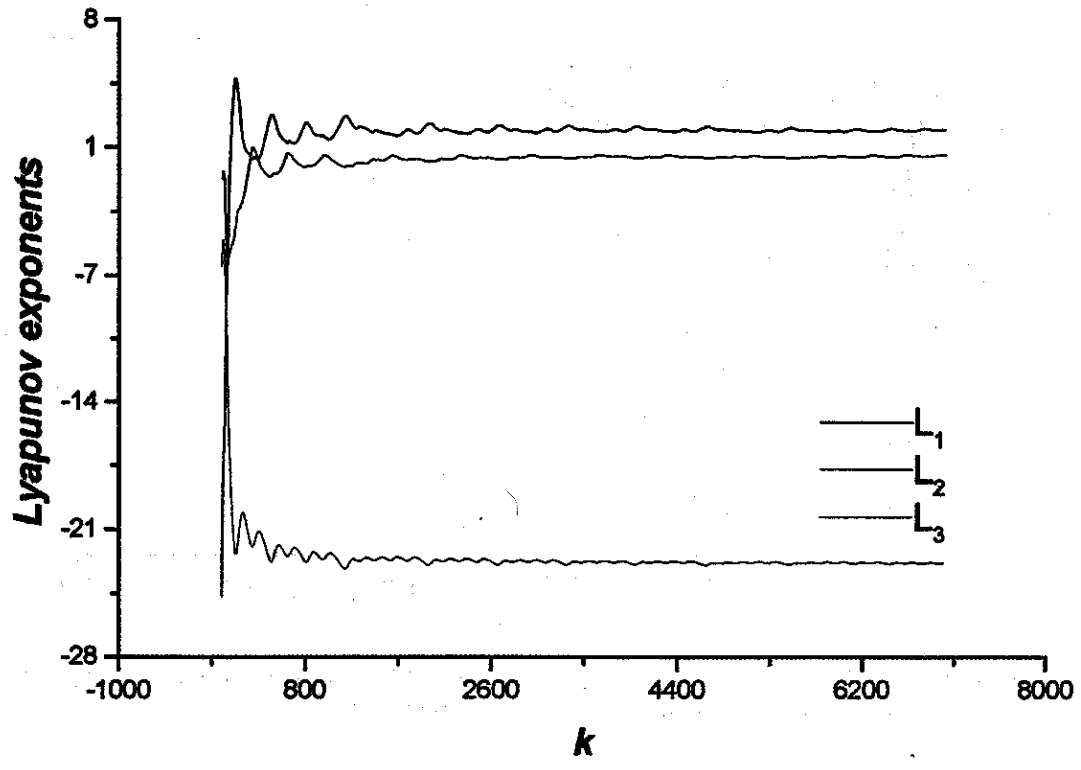

Fig. 13. A convergence of the Lyapunov exponents for the Lorenz equations.

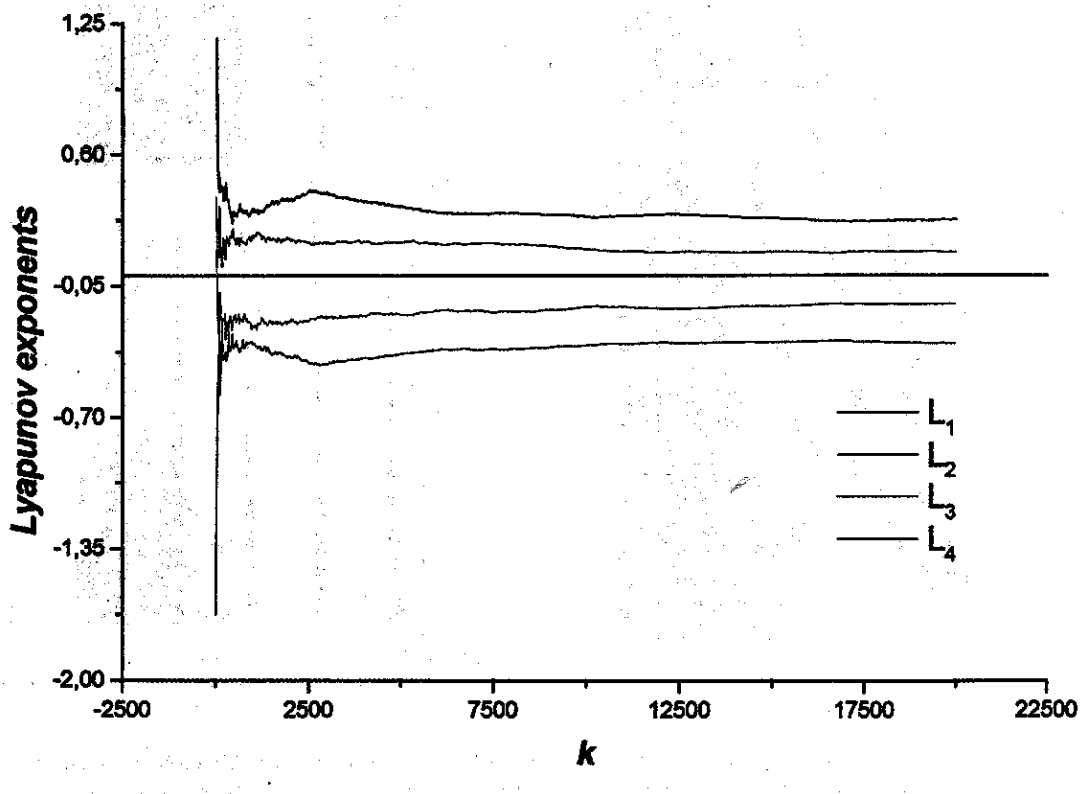

Fig. 14. A convergence of the Lyapunov exponents for the chaotic strange attractor illustrated in Fig. 9.

In Fig. 14, convergence is achieved after 1000 nondimensional time units. For the Lorenz system, similar convergence has been achieved after 280 (in both cases an accuracy was limited to two numbers after a dot). In spite of the approximation by the continuous function, the friction still possesses an essential influence on time needed to estimate the Lyapunov exponents.

4. Numerical Analysis and Results

4.1. *Algorithm*

The standard Runge–Kutta method with variable integration step has been used. Numerical experiments during investigation of our system have shown that very small Δt must be taken in order to make computational time more economical, and that Δt must be linked with the increase step of the variables Δy. In this work, it has been assumed that if Δy exceeds previously established δ value, then the program repeats the calculations using the Runge–Kutta method by using smaller Δt to obtain y_{n+1}. In the program, the Δt interval is increased according to the formula

$$\Delta t_{\text{new}} = \Delta t_{\text{old}} 0.95 \left(\frac{\delta}{\Delta y}\right)^{0.25}, \qquad (11)$$

whereas $\Delta y < \delta$, and is decreased according to the formula

$$\Delta t_{\text{new}} = \Delta t_{\text{old}} 0.95 \left(\frac{\delta}{\Delta y}\right)^{0.2}, \qquad (12)$$

for $\Delta y \geq \delta$.

4.2. *Results*

The computational results [Olejnik, 2000] are presented in Figs. 15–25.

Chaotic motions presented in Figs. 15 and 16 are similar to that exhibited by a sinusoidal excited pendulum. In Figs. 17 and 20, the phase planes together with the Poincaré maps (black squares) are presented. It is interesting to note (Fig. 17) that a special dynamics can be realized when one of the masses exhibits stick-slip periodic process, whereas

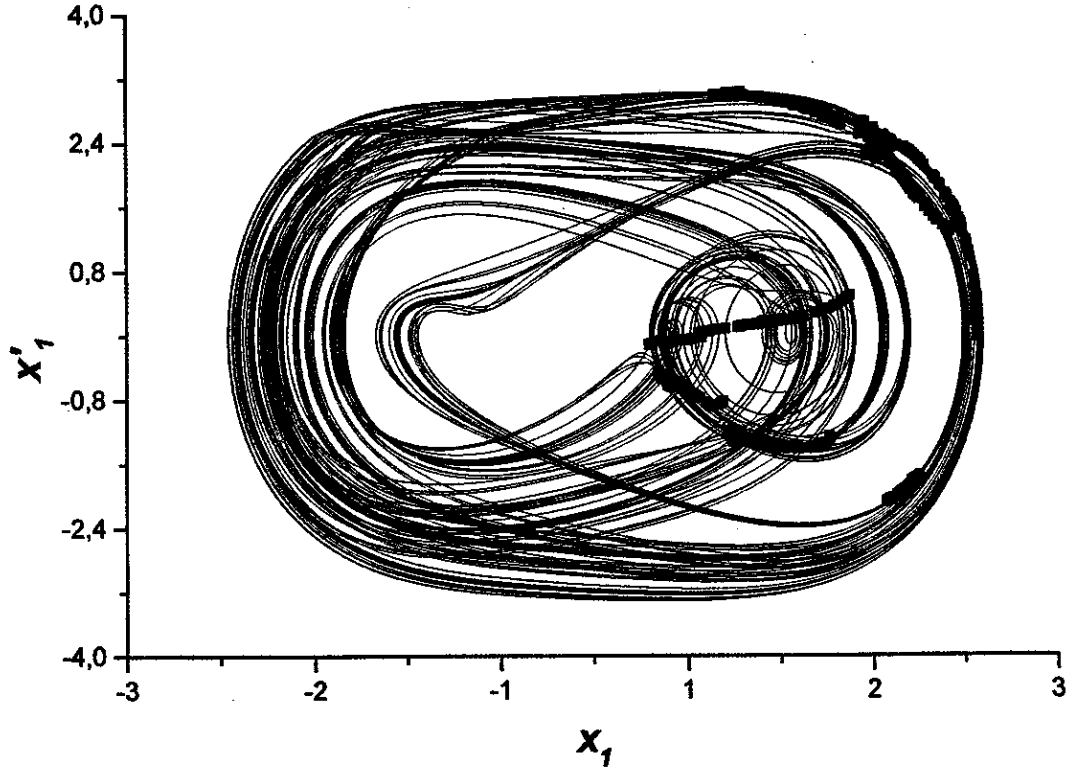

Fig. 15. Phase portrait and the corresponding Poincaré map (red points) $\dot{x}_1(x_1)$ for the parameters: $\gamma = 0.3$, $\beta = 1.7$, $V_0 = 2.5$, $\alpha_0 = 0$, $\alpha_1 = 0.002$, $\alpha_2 = 0.09$, $\beta_1 = 0.1$, $\beta_2 = 1.11$, $\xi_1 = 1$, $\xi_2 = 2.4$ and the initial conditions: $x_1 = -0.1$, $x_2 = 0.2$, $\dot{x}_1 = \dot{x}_2 = 0$ (chaotic orbit, Lyapunov exponents: 0.23, −0.01, −0.15, −0.28).

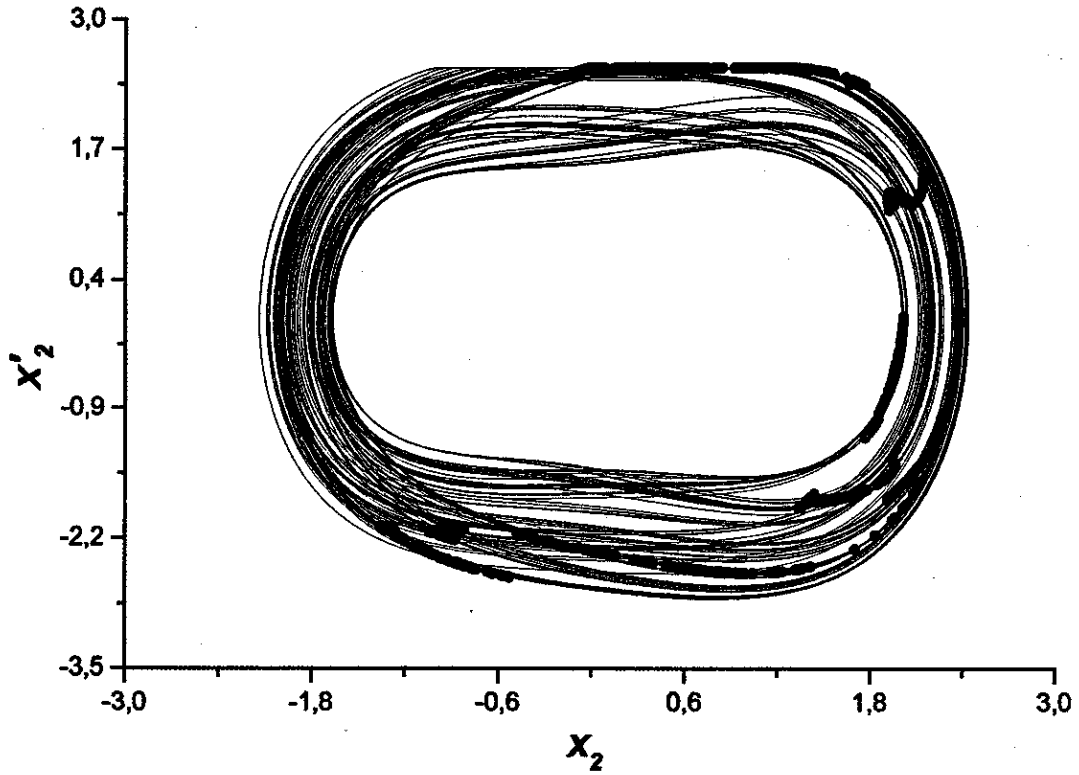

Fig. 16. Phase portrait and the corresponding Poincaré map (red points) $\dot{x}_2(x_2)$. Parameters are the same as in Fig. 15 (chaotic orbit).

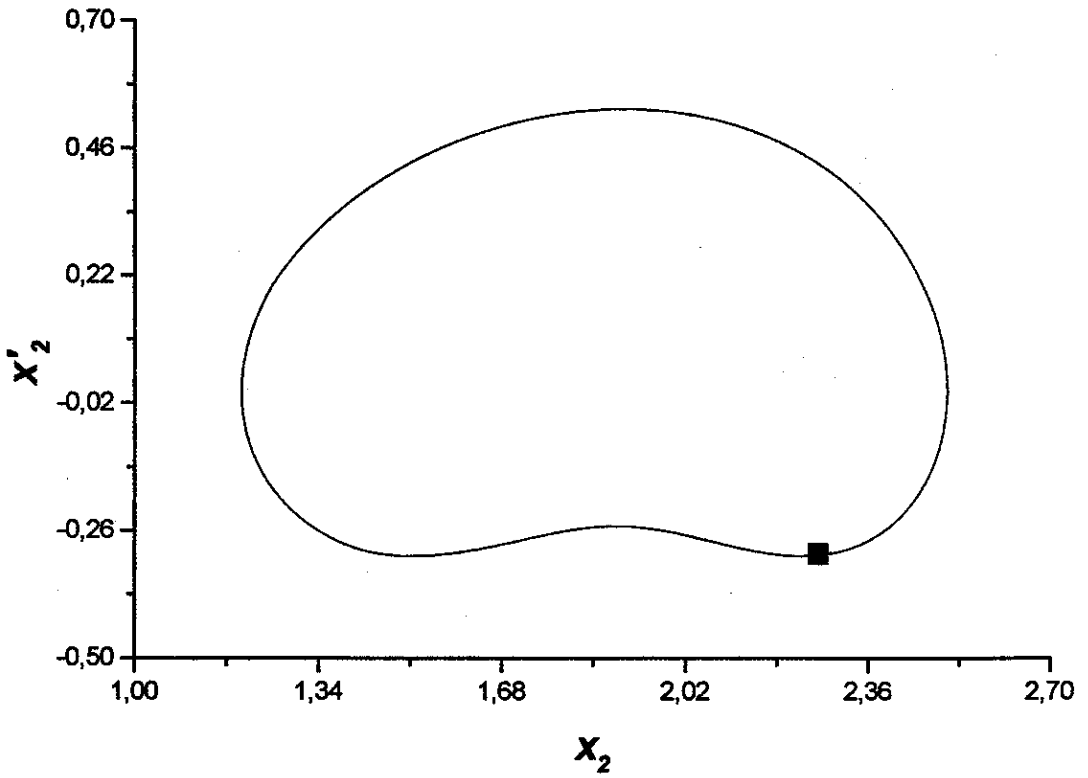

Fig. 17. Phase portrait and the corresponding Poincaré map (red square) $\dot{x}_2(x_2)$ for the parameters: $\gamma = 3$, $\beta = 0.04$, $V_0 = 0.2$, $\alpha_0 = 0.1$, $\alpha_1 = 0.03$, $\alpha_2 = 0$, $\beta_1 = 0.31$, $\beta_2 = 0.1$, $\xi_1 = 0.12$, $\xi_2 = 2$ and the initial conditions: $x_1 = x_2 = 0$, $\dot{x}_1 = 0.7$, $\dot{x}_2 = 0$ (periodic orbit, Lyapunov exponents: -0.01, -0.04, -0.19, -0.19).

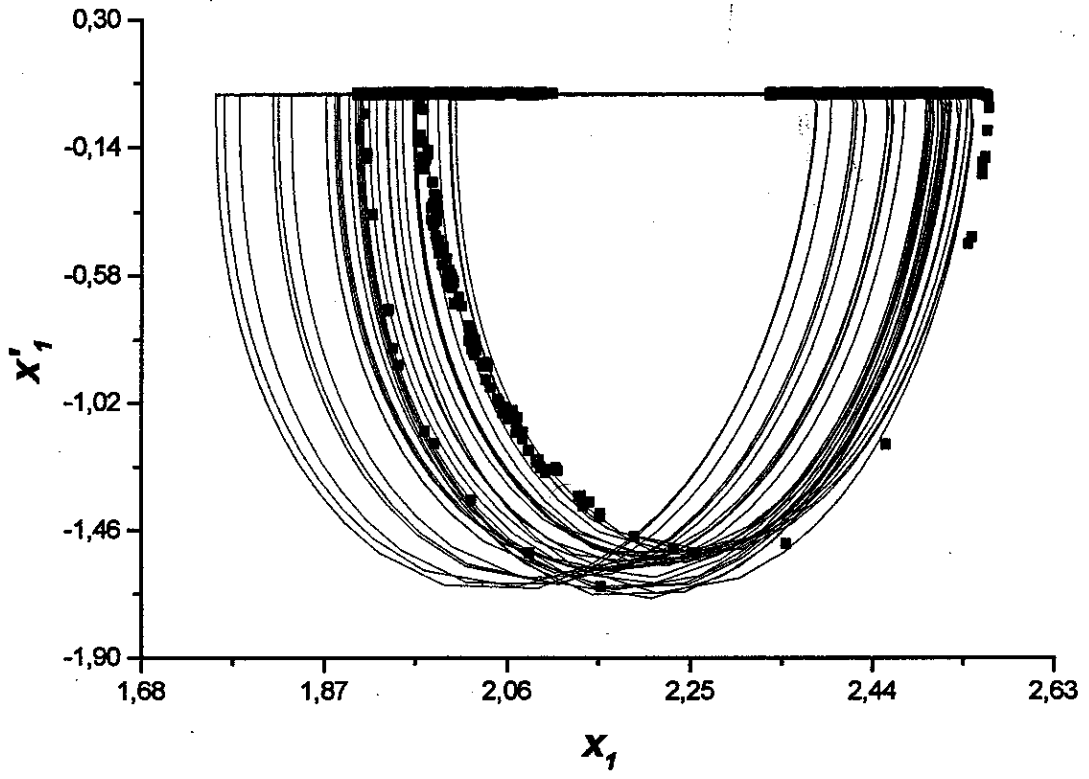

Fig. 18. Phase portrait and the corresponding Poincaré map (red square) $\dot{x}_1(x_1)$ for the parameters: $\gamma = 2.09$, $\beta = 0.984$, $V_0 = 0.043$, $\alpha_0 = 0.01$, $\alpha_1 = 0$, $\alpha_2 = 0.015$, $\beta_1 = 0.31$, $\beta_2 = 0.108$, $\xi_1 = 0.07$, $\xi_2 = 2.23$, and the initial conditions: $x_1 = x_2 = 0$, $\dot{x}_1 = 5$, $\dot{x}_2 = -5$ (chaotic orbit, Lyapunov exponents: 0.48, −0.08, −1.42, −6.31).

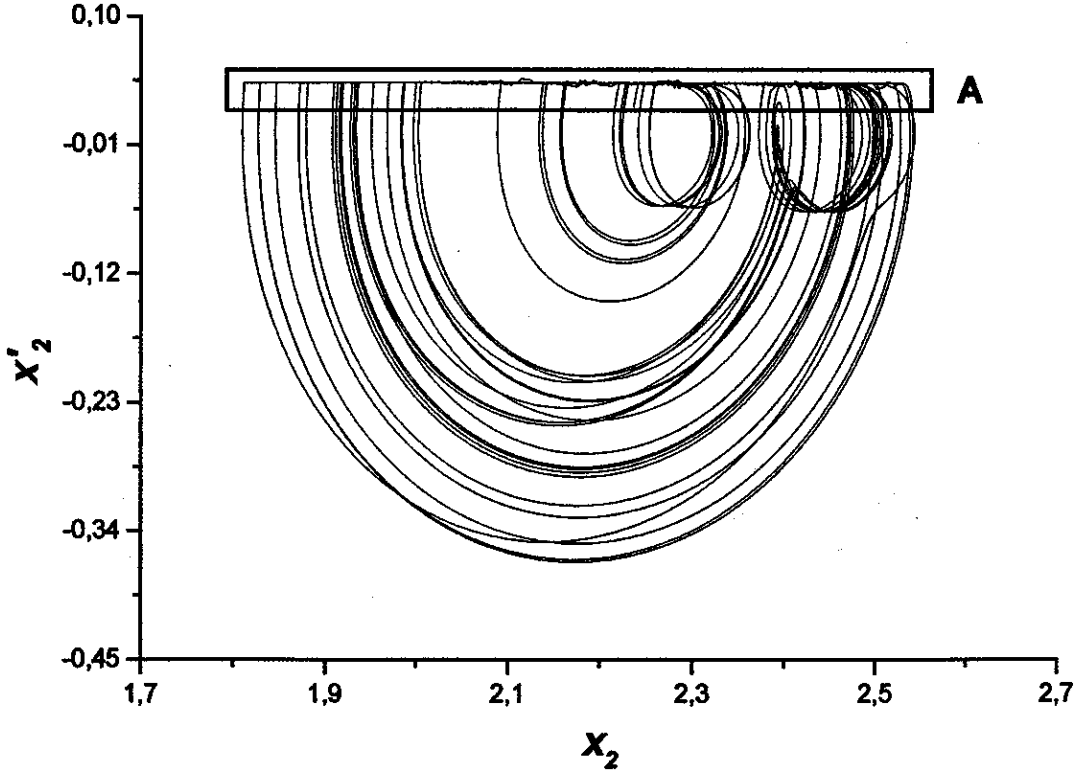

Fig. 19. Phase portrait $\dot{x}_2(x_2)$. Parameters are the same as in Fig. 18 (chaotic orbit).

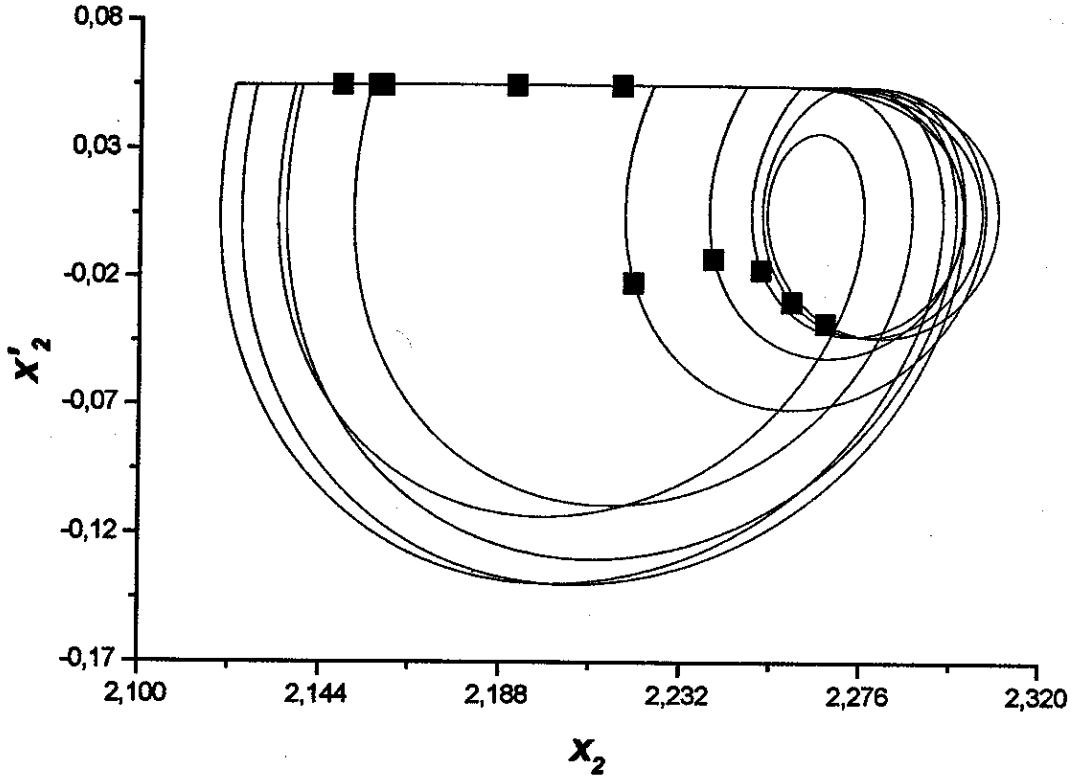

Fig. 20. Phase portrait and the corresponding Poincaré map (red square) $\dot{x}_2(x_2)$ for the parameters: $\gamma = \beta = 1$, $V_0 = 0.05$, $\alpha_0 = \alpha_1 = \alpha_2 = 0.03$, $\beta_1 = \beta_2 = 0.1$, $\xi_1 = 0.12$, $\xi_2 = 1$ and the initial conditions: $x_1 = 0.4$, $x_2 = -0.12$, $\dot{x}_1 = -0.56$, $\dot{x}_2 = 0.12$ (periodic orbit, Lyapunov exponents: -0.16, -0.17, -0.31, -0.33).

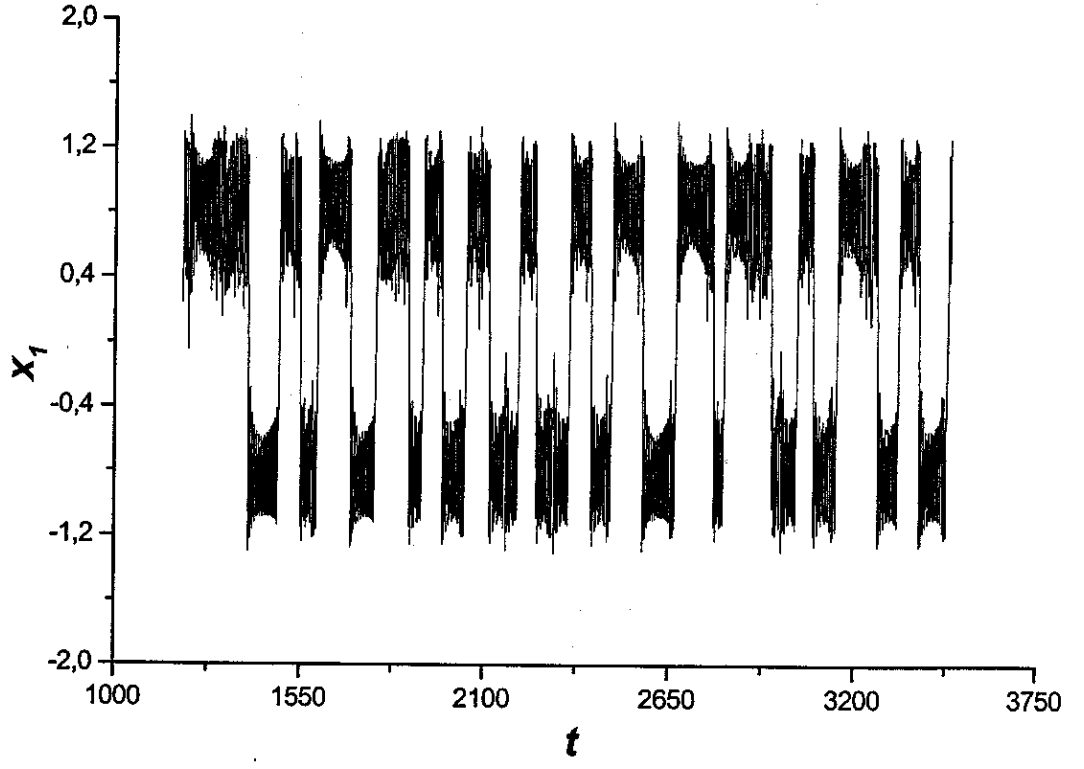

Fig. 21. Phase portrait $\dot{x}_2(x_2)$. Parameters are the same as in Fig. 18 (chaotic orbit).

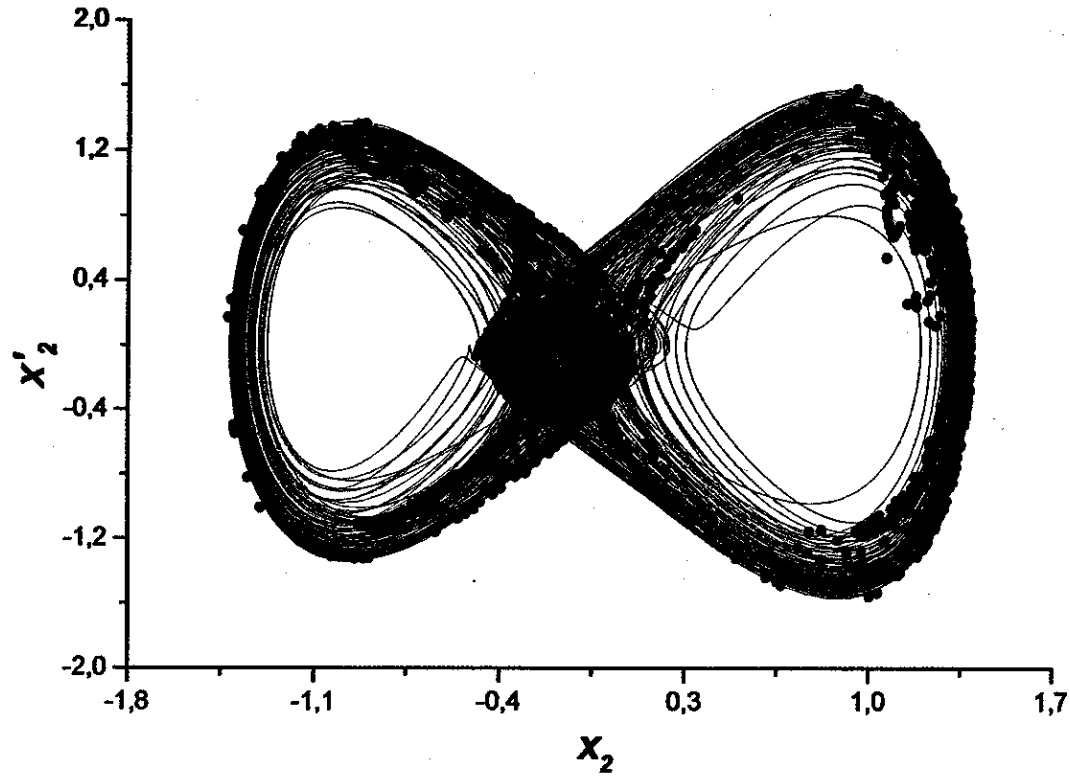

Fig. 22. Phase portrait and the corresponding Poincaré map (red points) $\dot{x}_2(x_2)$. Parameters and initial conditions are the same as in Fig. 21 (chaotic orbit, Lyapunov exponents: 0.36, 0.21, −0.42, −0.43).

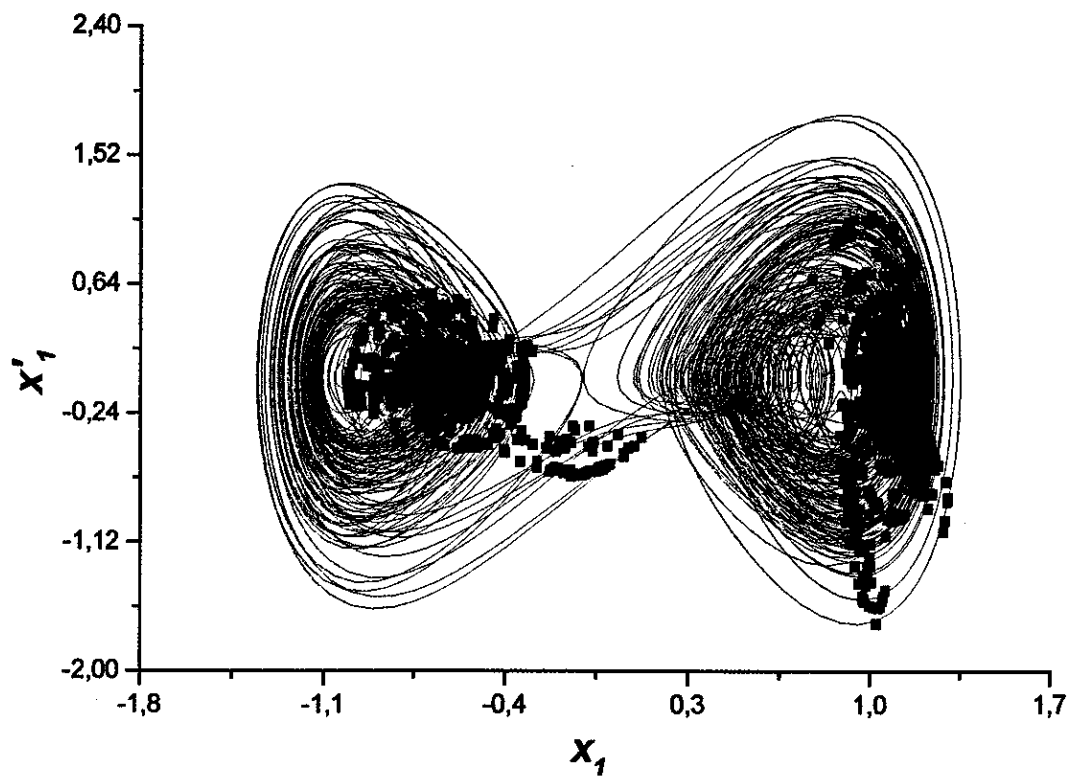

Fig. 23. Phase portrait and the corresponding Poincaré map (red points) $\dot{x}_1(x_1)$. Parameters and initial conditions are the same as in Fig. 21 (chaotic orbit).

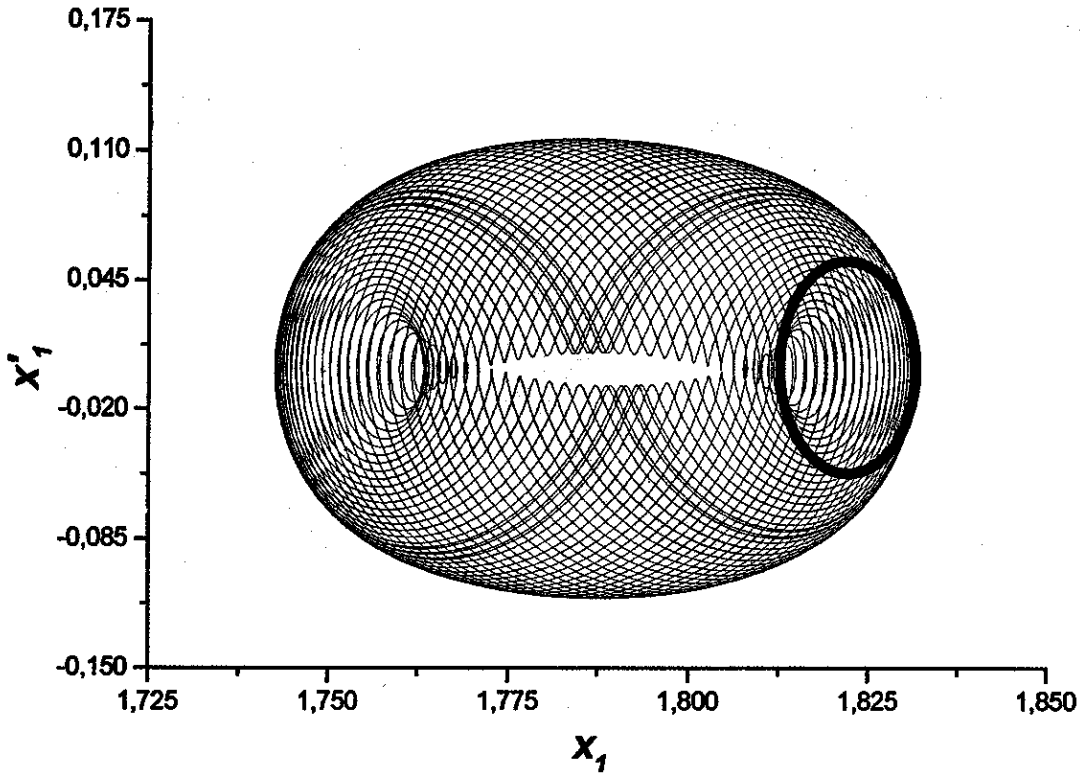

Fig. 24. Phase portrait and the corresponding Poincaré map (red circle) $\dot{x}_1(x_1)$ for the parameters: $\gamma = 0.03$, $\beta = 0.77$, $V_0 = 0.2$, $\alpha_0 = 0$, $\alpha_1 = 0.01$, $\alpha_2 = 0$, $\beta_1 = 0.12$, $\beta_2 = 0.2$, $\xi_1 = 0.1$, $\xi_2 = 0.7$ and the initial conditions: $x_1 = 0$, $x_2 = 0.2$, $\dot{x}_1 = \dot{x}_2 = 0$ (quasi-periodic orbit, Lyapunov exponents: -0.00, -0.03, -0.20, -0.20).

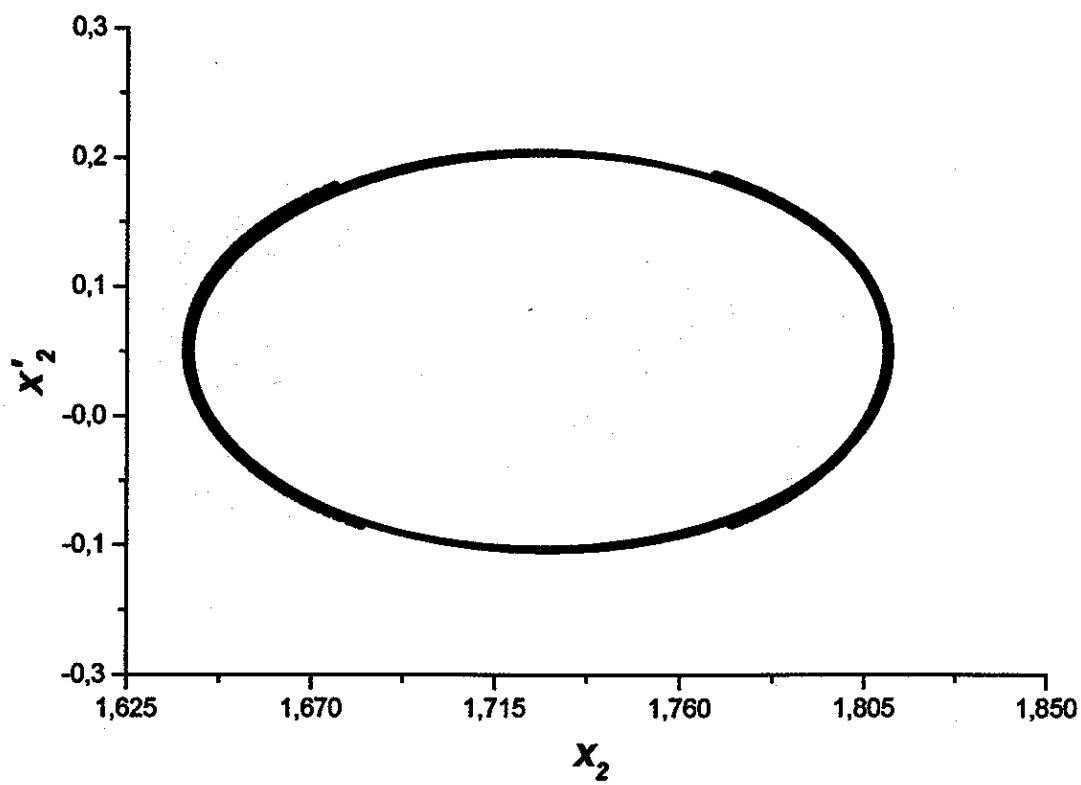

Fig. 25. Phase portrait and the corresponding Poincaré map (red lines) $\dot{x}_2(x_2)$. Parameters are the same as in Fig. 24 (quasi-periodic orbit).

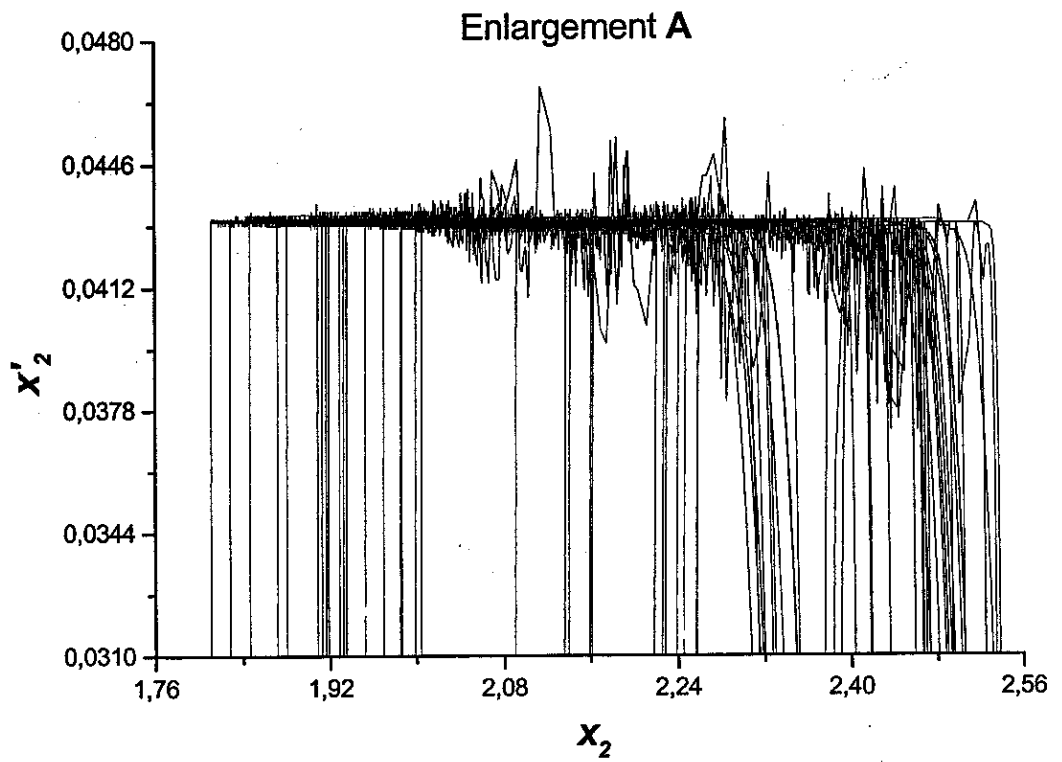

Fig. 26. Oscillations of the mass m_2.

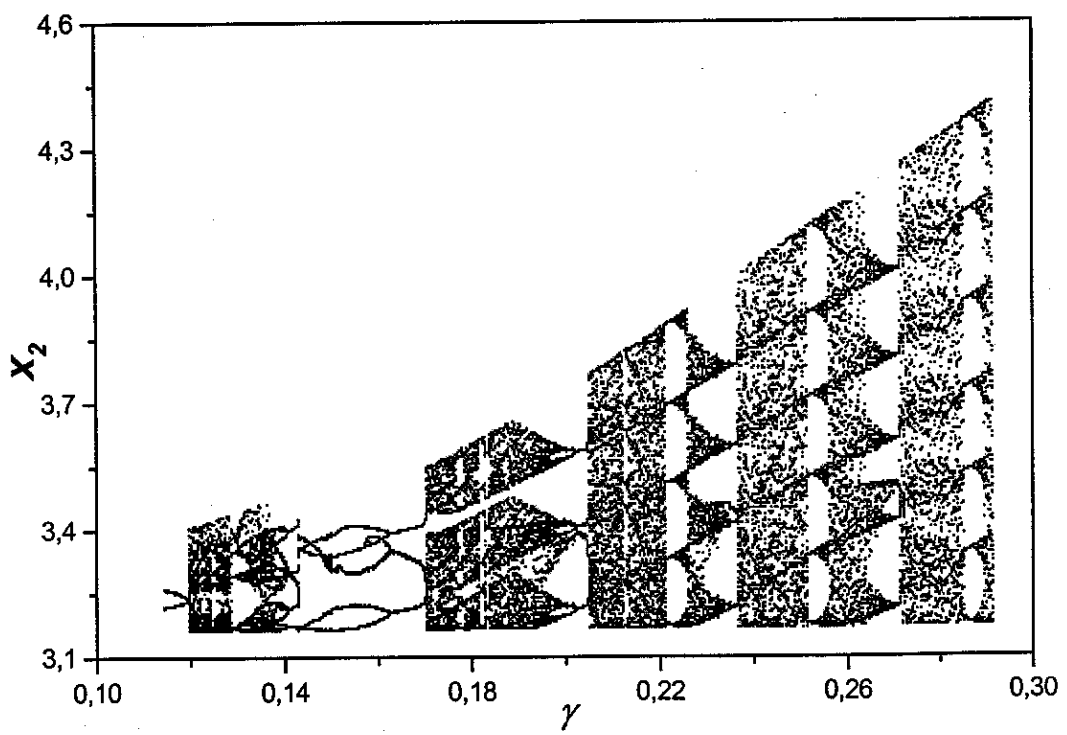

Fig. 27. Bifurcation diagram for the parameter $\gamma \in (0.2, 0.4)$. The following parameters are fixed: $\beta = 1$, $V_0 = 3$, $\alpha_0 = 0.003$, $\alpha_1 = 0.05$, $\alpha_2 = 0$, $\beta_1 = 0.2$, $\beta_2 = 2.34$, $\xi_1 = 0.45$, $\xi_2 = 0.76$ and the initial conditions: $x_1 = 1$, $x_2 = -2.32$, $\dot{x}_1 = -0.78$, $\dot{x}_2 = 3$.

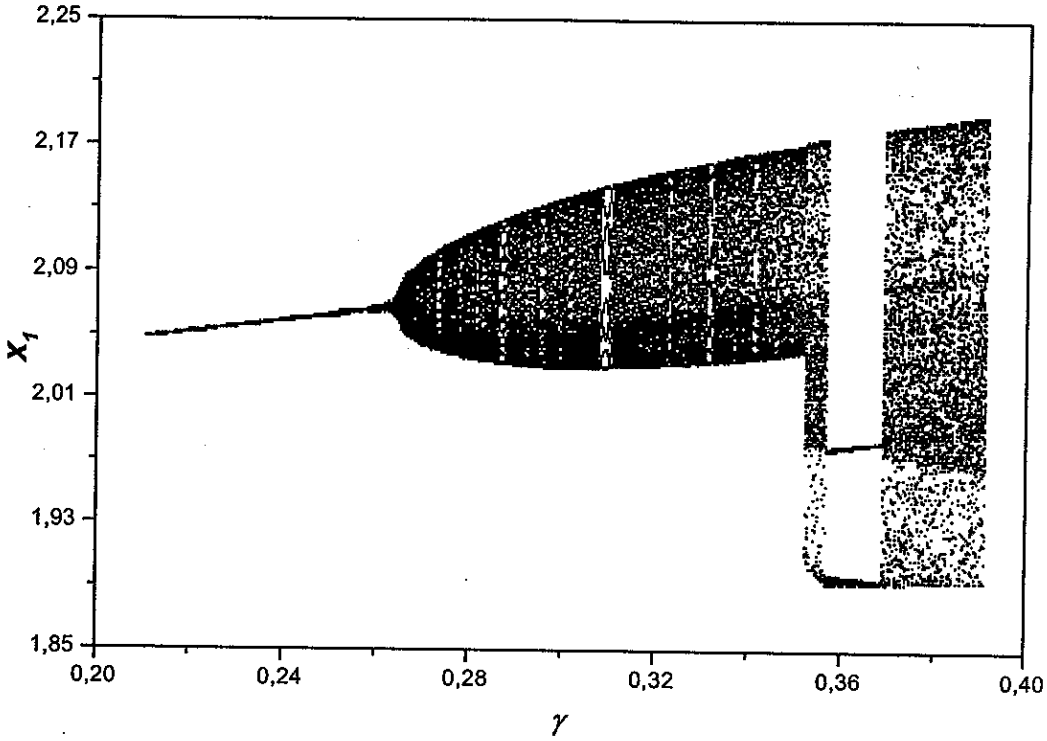

Fig. 28. Bifurcation diagram for the parameter $\gamma \in (0.1, 0.3)$. The following parameters are fixed: $\beta = 21$, $V_0 = 0.2$, $\alpha_0 = 0.0045$, $\alpha_1 = 0.01$, $\alpha_2 = 0.19$, $\beta_1 = 0.12$, $\beta_2 = 0.2$, $\xi_1 = 0.1$, $\xi_2 = 0.7$ and the initial conditions: $x_1 = -0.1$, $x_2 = 0.2$, $\dot{x}_1 = \dot{x}_2 = 0$.

the second only the slip one. In Fig. 20, an example of very complicated stick-slip periodic behavior is reported. Figures 18 and 19 illustrate a stick-slip chaos, which has been achieved via period doubling bifurcations.

This example contains even more information, when one starts to trace moments of sticks for the mass m_2 (see enlargement given in Fig. 26). It is seen how complicated dynamics can occur during stick-slip processes. In Fig. 22, the time histories of masses and chaotic motions are reported. For this case, we have hyperchaotic dynamics because two of the Lyapunov exponents are positive and the Lyapunov dimension $d_L = 2.35$ testifies the chaotic attractor as the strange one. In addition, both masses move in a different manner: the mass m_1 jumps between two potential wells very quickly, whereas the second mass m_2 exhibits similar jumps, which occur slowly. The quasi-periodic motion is presented in Figs. 24 and 25. The mass m_1 moves on a tours, but the Poincaré map associated with the second mass possesses two symmetric arc form attractors.

Finally, we give two examples of bifurcation diagrams. Among others, it is shown that the analyzed system with friction exhibits simple bubbles (Fig. 27) for $\gamma \approx 0.14$. Another bifurcation diagram, which is rather typical for a simple dynamical system, is presented in Fig. 28. Both show many jumps between periodic and chaotic attractors, and vice versa.

5. Concluding Remarks

The classical two-degree-of freedom self-excited system with friction has been analyzed using numerical methods. The original program using Visual C++ 6.0 has been prepared. The main purpose of this work has been focused on analysis of stick-slip regular (periodic and quasi-periodic) and chaotic dynamics. Another goal was to apply smoothing procedure to model discontinuous friction using arc tan function. It possesses two main advantages. (1) Slightly modified Runge–Kutta method with variable integration step can be used (during stick phase a larger integration step is recommended). (2) The smoothness introduced by arc tan allowed to use classical tools of nonlinear dynamics, and to keep all behavior related to discontinuous effects. The sgn function is not defined when the

relative velocity is equal to zero, whereas the arc tan is a unique function yielding both stick and slip phenomena.

During the analysis, all standard techniques have been applied, i.e. time histories, phase planes, Poincaré maps, the Lyapunov exponents and the Lyapunov dimensions.

Very rich nonlinear nonsmooth dynamics has been detected. The period doubling route to stick-slip chaos, and from stick-slip chaos to regular motion (Fig. 27), very complicated stick-slip periodic orbits (Fig. 20), stick-slip hyper-chaos (Figs. 9, 21–23), various quasi-periodic attractors (Figs. 11, 24 and 25), as well as different seemingly periodic motions exhibited by the masses, i.e. stick-slip and smooth periodic orbits (Figs. 3, 6, 10 and 17) have been discussed and illustrated.

In addition, the numerical simulations indicate how complicated nonlinear dynamics occurs during the stick-slip processes (Fig. 26).

Acknowledgment

This work has been supported by the Polish State Committee for Scientific Research (Grant No. 5T07A01923).

References

Awrejcewicz, J. & Mrozowski, J. [1989] "Bifurcations and chaos of particular Van der Pol Duffing oscillator," *J. Sound Vib.* **132**(1), 89–100.

Awrejcewicz, J. & Delfs, J. [1990a] "Dynamics of a self-excited stick-slip oscillator with two degrees of freedom, Part I, Investigation of equilibria," *European J. Mech. A/Sol.* **9**(4), 269–282.

Awrejcewicz, J. & Delfs, J. [1990b] "Dynamics of a self-excited stick-slip oscillator with two degrees of freedom. Part II, Slip-stick, slip-slip, stick-slip transitions, periodic and chaotic orbits," *European J. Mech. A/Sol.* **9**(5), 397–418.

Awrejcewicz, J. [1996] *Deterministic Oscillations of Discrete Systems* (WNT, Warsaw) (in Polish).

Awrejcewicz, J. & Holicke, M. M. [1999] "Melnikov's method and stick-slip chaotic oscillations in very weakly forced mechanical systems," *Int. J. Bifurcation and Chaos* **9**(3), 505–518.

Brogliato, B. [1996] *Nonsmooth Impact Mechanics* (Springer-Verlag, London).

Deimling, K. & Szilágyi, P. [1994] "Periodic solutions of dry friction problems," *Z. Angew. Math. Phys.* **45**, 53–60.

Feeny, B. F. & Moon, F. C. [1989] "Autocorrelation on symbol dynamics for a chaotic dry friction oscillator," *Phys. Lett.* **A41**(8&9), 397–400.

Galvanetto, U., Bishop, R. S. & Briseghella, L. [1995] "Some remarks on the stick-slip vibrations of a two-degree-of-freedom mechanical model," *Mech. Rev. Commun.* **20**(6), 459–466.

Grabec, I. [1986] "Chaos generated by the cutting process," *Phys. Lett.* **A117**, 236–384.

Jayaraman, K. [1991] "Chaotic vibrations of some nonlinear mechanical systems," Ph.D. thesis, Indian Institute of Technology, Madras.

Kunze, M. [2000] *Non-Smooth Dynamical System*, Lecture Notes in Mathematics, Vol. 1744 (Springer Verlag, Berlin).

Monteiro Marques, M. D. P. [1994] "An existence, uniqueness and regularity study of the dynamics of systems with one-dimensional friction," *European J. Mech. A/Sol.* **13**(2), 277–306.

Narayanan, S. & Jayaraman, K. [1989] "Chaotic motions in nonlinear systems with Coulomb damping," *Proc. IUTAM Symp. Nonlinear Dynamics in Engineering Systems*, ed. Schiehlen, W. (Springer-Verlag, Berlin), pp. 217–224.

Oden, J. T. & Martins, J. C. A. [1985] "Models and computational methods for dynamics friction phenomena," *Comp. Met. App. Mech. Eng.* **52**, 527–634.

Olejnik, P. [2000] *Regular and Chaotic Dynamics of the Two-Degree-of-Freedom System*, Master Thesis, (in Polish).

Oseledec, V. I. [1968] "A multiplicative ergodic theorem: Lyapunov characteristic numbers for dynamical systems," *Trans. Moscow Math. Soc.* **19**, 197–231.

Popp, K. & Stelter, P. [1989] "Nonlinear oscillations of structures induced by dry friction," *Proc. IUTAM Symp. Nonlinear Dynamics and Engineering Systems*, ed. Schiehlen, W. (Springer-Verlag, Berlin), pp. 233–240.

Pratt, T. K. & Williams, R. [1981] "Nonlinear analysis of stick-slip motion," *J. Sound Vib.* **74**(4), 531–542.

Van de Vrande, B. L., Van Campen, D. H. & De Kraker, A. [1999] "An approximate analysis of dry-friction-induced stick-slip vibrations by a smoothing procedure," *Nonlin. Dyn. Chaos* **19**, 157–169.

Wolf, A., Jack, B., Swinney, H. L. & Vastano, J. A. [1985] "Determining Lyapunov exponents from a time series," *Physica* **D16**, 285–317.